Theoretical and numerical investigation of the impact of out-of-plane compressive stress on sheet metal formability

Mohamed Ben Bettaieb, Farid Abed-Meraim

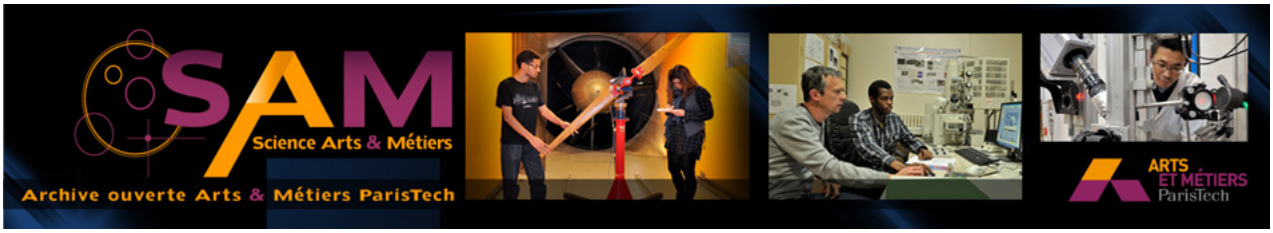

Theoretical and numerical investigation of the impact of out-of-plane compressive stress on sheet metal formability

M. Ben Bettaieb [a], F. Abed-Meraim [b,*]

[a] Laboratoire d'Étude des Microstructures et de Mécanique des Matériaux (LEM3), UMR 7239, CNRS/Arts et Métiers ParisTech, 4 rue Augustin Fresnel, 57078 Metz Cedex 3, France
[b] DAMAS, Laboratory of Excellence on Design of Alloy Metals for low-mAss Structures, Université de Lorraine, Metz, France

A B S T R A C T

In modern sheet metal forming processes, such as hydroforming and single point incremental forming, sheet metals are often subjected to out-of-plane compressive stresses in addition to traditional in-plane stresses. However, the effect of these out-of-plane stresses on the onset of plastic strain localization is not considered when classic necking criteria are used, as the latter are generally formulated based on the plane stress assumption. The main objective of the present investigation is to overcome this limitation by developing numerical tools and analytical relations that allow considering the influence of these compressive stresses on the prediction of localized necking. In the different tools developed, and for comparison purposes, finite strain versions of both the deformation theory of plasticity and the rigid-plastic flow theory are used to describe the mechanical behavior of the metal sheet. Furthermore, both the bifurcation theory and the initial imperfection approach are employed to predict the onset of strain localization. Various numerical predictions are reported to illustrate the effect of normal stress on the occurrence of localized necking in sheet metals. From these different results, it is clearly demonstrated that out-of-plane stresses may notably enhance sheet metal formability and, therefore, this property can be effectively used to avoid the initiation of early strain localization.

1. Introduction

The localization of deformation is often regarded as one of the most detrimental defects encountered in sheet metal forming operations. This phenomenon is considered as the main factor that limits the formability of sheet metals. To evaluate this ductility limit, the concept of forming limit diagram (FLD), originally developed in the pioneering work of Keeler and Backofen [1], has been widely employed. Because the experimental procedures for estimating the forming limit strains reveal to be time consuming and costly, various analytical and/or numerical models and tools have been set up to predict the occurrence of strain localization, among which the bifurcation theory [2], Marciniak and Kuczynski's analysis [3], and the perturbation approach [4]. In most cases, these different theoretical models are based on the plane stress assumption. Although justified for most press-forming operations, where the critical portion of the sheet is almost free from out-of-plane forces at both sides of its surface, this plane stress assumption should not be generalized. Indeed, in some modern sheet metal forming operations, such as hydroforming and incremental forming processes, non-zero normal and through-thickness stresses may be observed. In the current contribution, attention is restricted to the effect of normal compressive stress on sheet metal formability, while the impact of out-of-plane shear stresses is disregarded. This assumption is motivated by the low magnitude of these out-of-plane shear stresses, as compared to the magnitude of the classic out-of-plane compressive stress observed in real sheet metal forming processes. Indeed, in the case of hydroforming process, the out-of-plane shear stresses are identically equal to zero and only the stress component normal to the sheet is different from zero. In other forming processes, such as deep-drawing, through-thickness shear stresses arise most commonly from the friction between the sheet and the tool. Hence, when friction is considered, these through-thickness shear stresses are proportional to the pressure normal to the plane of the sheet by a factor much smaller than unity in most sheet forming applications. Since frictional effects are usually purposely minimized in these forming applications, they are expected to be an order of magnitude smaller than the contact pressure in typical manufacturing processes, where the friction coefficient is of the order of 0.1, and the maximum through-thickness shear stresses would be expected to be of the order of 10% of the out-of-plane compressive stress. Therefore, it makes sense to consider the case of non-zero normal stress along with zero through-thickness shear stresses as a first good approximation before considering the more general case of fully three-dimensional stress conditions. In this context, several au-

thors have extended some strain localization criteria to account for the effect of stress component, along the normal to the sheet plane, on the prediction of FLDs. In this regard, one may quote Gotoh et al. [5], who extended both the Swift criterion [6] and the Hill criterion [7] to a 3D stress state, so as to investigate the effect of normal stress on the onset of diffuse and localized necking, respectively. More recently, Allwood and Shouler [8] have extended the Marciniak and Kuczynski approach to account for the effect of normal stress component on the predicted limit strains. In this latter analysis, an isotropic rigid-plastic flow theory has been used to describe the mechanical behavior of the studied sheet. As a result of this earlier investigation, a new generalized forming limit diagram has been proposed, which highlights the influence of normal stress component on the formability limit. Note that a specifically designed linear paddle testing apparatus has been used in [9] to experimentally assess the increase in formability limits due to the application of normal compressive stresses. It is shown in this latter study that the use of simplifying assumptions, such as plastic isotropy, results in some discrepancies between numerical predictions and experimental results. To avoid this drawback, Fatemi and Dariani [9] extended the approach developed in [8], by taking into account the plastic anisotropy of the sheet via the application of Hill'48 yield criterion. Another extension of the Marciniak and Kuczynski approach has been developed in [10]. This extension has been validated on the basis of several experimental results for AA6011 and STKM-11A materials. Note also that, within the Marciniak and Kuczynski approach, the effect of through-thickness normal stress on the forming limits has been investigated using other yield criteria (see, e.g., [11,12], where the Barlat and the YLD2003 yield criteria have been used, respectively). More recently, the concepts of stress-based forming limit diagram (FLSD) and extended forming limit stress diagram (XFLSD) have been adopted in [13] to investigate the effect of through-thickness normal stress on the formability limit. For all of these studied materials, the numerical predictions are found to be quantitatively consistent with the available experimental results.

Building on this insight, the current paper aims to develop an extension of some numerical tools, while accounting for the effect of the stress component along the direction normal to the sheet plane. These numerical tools have been originally developed in [14] and recently revisited and improved in [15]. In these tools, two main strain localization criteria have been used to predict the occurrence of localized necking: the bifurcation theory and the Marciniak and Kuczynski approach (also referred to as the initial imperfection approach). As previously assumed, the impact of out-of-plane shear stresses (and consequently out-of-plane shear strains) on the formability prediction is neglected. Therefore, a 2D formulation can be followed to formulate the bifurcation theory and the initial imperfection approach. In this case, the set of governing equations can be expressed in the plane of the sheet and the necking band remains normal to the sheet plane during the straining. Such a formulation is very similar to the one used when the plane stress state is assumed. Consequently, the predictions obtained with the application of non-zero normal compressive stress can be naturally compared with predictions obtained under the plane stress assumption. In situations when the out-of-plane shear stress components cannot be neglected, this simple 2D (plane) formulation cannot be preserved any more, and the prediction of localized necking becomes a relatively complex task [16]. In the current work, each of the above-discussed strain localization approaches has been coupled with two constitutive frameworks, namely a rigid-plastic finite strain version of the J_2 deformation theory of plasticity (shortly designated in what follows as "deformation theory") and of the J_2 flow theory of plasticity (shortly called hereafter "flow theory"). The major conclusion of the present investigation is that the presence of positive compressive stress, normal to the sheet plane, may substantially delay the onset of localized necking. It is also shown that the limit strains predicted by the initial imperfection approach tend towards those computed by the bifurcation theory, when the size of the geometric imperfection tends towards zero.

The remainder of the paper is structured as follows:

- Section 2 provides a short description of the different constitutive frameworks, which are adopted for the modeling of the mechanical behavior of the studied sheet metal.
- Section 3 details the main equations on which the different localization criteria are based.
- In Section 4, the influence of constant normal stress on the occurrence of localized necking is emphasized through various numerical predictions and results. The effect of variable normal stress on formability is analyzed in Appendix B.

Notations, conventions and abbreviations

The list of notations, conventions and abbreviations used in this paper are clarified in the box bellow. Additional notations will be provided when needed.

Bold letters are used to represent vector and tensor variables.
Thin letters are used to represent scalar variables and parameters.
Einstein's summation convention is used.
The range of the dummy (resp. free) index is given after (resp. before) the corresponding equation.

$\dot{\bullet}$	derivative of $\bullet$ with respect to time
$\mathbf{I}_2$	second-order identity tensor
$\vec{\bullet}\otimes\vec{\bullet}$	tensor product of two vectors ($=\bullet_i\bullet_j$)
$\bullet_I$	quantity $\bullet$ evaluated at the initial time
$\tilde{\bullet}$	in-plane part of vector or second-order tensor $\bullet$ defined as $(\bullet_1\ \bullet_2)$ or $\begin{pmatrix}\bullet_{11} & \bullet_{12}\\ \bullet_{21} & \bullet_{22}\end{pmatrix}$, respectively
$\coth(\bullet)$	hyperbolic cotangent of $\bullet$
$\bullet^B$	quantity $\bullet$ within the band
$\bullet^S$	quantity $\bullet$ within the safe zone

2. Constitutive equations

As previously stated, for the sake of comparison, the investigations carried out in the present paper adopt two constitutive frameworks: the flow theory of plasticity and the total deformation theory.

2.1. Flow theory

The elasticity of the sheet metal is neglected. This choice is justified by the fact that strain localization occurs at relatively large strains. Hence, the mechanical behavior of the material is modeled by an associative rigid-plastic flow theory. Accordingly, the normality flow rule is used to obtain the expression of the strain rate tensor $\dot{\boldsymbol{\varepsilon}}$ (the symmetric part of the velocity gradient $\mathbf{G}$)

$$\dot{\boldsymbol{\varepsilon}} = \dot{\varepsilon}_{eq}\frac{\partial\sigma_{eq}}{\partial\boldsymbol{\sigma}}, \tag{1}$$

where:

$\dot{\varepsilon}_{eq}$ is the equivalent strain rate.
σ_{eq} is the equivalent stress.
$\boldsymbol{\sigma}$ is the Cauchy stress tensor.

Furthermore, plasticity is assumed to be isotropic and the von Mises criterion is used to predict material yielding. Consequently, the equivalent strain rate and stress measures $\dot{\varepsilon}_{eq}$ and σ_{eq} are related to tensors $\dot{\boldsymbol{\varepsilon}}$ and $\boldsymbol{\sigma}$ by the following relations, respectively:

$$\dot{\varepsilon}_{eq} = \sqrt{(2/3)\,\dot{\boldsymbol{\varepsilon}} : \dot{\boldsymbol{\varepsilon}}}; \quad \sigma_{eq} = \sqrt{(3/2)\,\mathbf{S} : \mathbf{S}}, \tag{2}$$

where $\mathbf{S}$ is the deviatoric part of $\boldsymbol{\sigma}$.

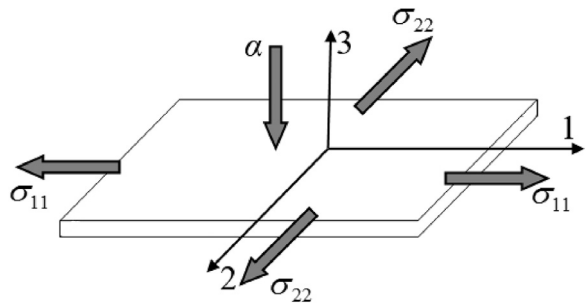

Fig. 1. Schematic representation of the loading applied to a small element of the sheet.

By substituting Eq. (2) into Eq. (1), the normality rule can be equivalently rewritten as

$$\dot{\boldsymbol{\varepsilon}} = \frac{3}{2}\frac{\dot{\varepsilon}_{eq}}{\sigma_{eq}}\mathbf{S} \Leftrightarrow \mathbf{S} = \frac{2}{3}\frac{\sigma_{eq}}{\dot{\varepsilon}_{eq}}\dot{\boldsymbol{\varepsilon}}. \tag{3}$$

On the other hand, the equivalent strain ε_{eq} is related to the equivalent stress σ_{eq} by the Hollomon hardening law

$$\sigma_{eq} = K\,\varepsilon_{eq}^{n} \quad \textit{where} \quad \varepsilon_{eq} = \int_0^t \dot{\varepsilon}_{eq}\,\mathrm{d}t, \tag{4}$$

with n and K being hardening parameters.

2.2. Deformation theory

The constitutive equations governing the J_2 deformation theory of plasticity have been initially formulated in the frame of the principal strain directions. This original formulation is restricted to isotropic materials [14], where the frame of principal strain directions is aligned with that of principal stress directions. In this formulation, the logarithmic strains ϵ_i and the principal deviatoric stresses S_i are related by the following equation:

$$\forall\, i = 1,2,3: \quad S_i = \frac{2\,\sigma_{eq}}{3\,\varepsilon_{eq}}\epsilon_i. \tag{5}$$

Eq. (5) has been subsequently generalized in [15] to a tensor form, which is valid for any coordinate system

$$\mathbf{S} = \frac{2}{3}\,E_S\,\ln\mathbf{V}, \tag{6}$$

where E_S and $\ln\mathbf{V}$ are the secant modulus and the natural logarithmic of the left Cauchy–Green stretch tensor $\mathbf{V}$, respectively. The secant modulus E_S is defined as

$$E_S = \frac{\sigma_{eq}}{\varepsilon_{eq}}. \tag{7}$$

Similar to the case of flow theory, hardening is modeled by the Hollomon law. Accordingly, the secant modulus E_S is obtained by inserting Eq. $(4)_1$ into Eq. (7), which gives

$$E_S = K\,\varepsilon_{eq}^{n-1}. \tag{8}$$

2.3. Consideration of non-zero constant normal stress

The studied sheet is subjected to biaxial stretching in the 1 and 2 directions (Fig. 1). Additionally, a non-zero principal stress σ_{33} $(=-\alpha)$ acts in the out-of-plane direction (i.e., in the 3-direction), where α is assumed to be a non-negative constant pressure. The validity of this assumption (constant pressure) has been proven in the case of hydroforming processes (see, e.g., [17,18]). This pressure is also assumed to be uniformly distributed within the plane and the thickness of the sheet.

Under these loading conditions, the Cauchy stress tensor $\boldsymbol{\sigma}$ can be expressed as follows:

$$\boldsymbol{\sigma} = \begin{pmatrix} \sigma_{11} & 0 & 0 \\ 0 & \sigma_{22} & 0 \\ 0 & 0 & -\alpha \end{pmatrix}. \tag{9}$$

Tensor $\boldsymbol{\sigma}$ is related to its deviatoric part $\mathbf{S}$ by

$$\begin{aligned} \mathbf{S} &= \boldsymbol{\sigma} - (1/3)\,tr(\boldsymbol{\sigma})\,\mathbf{I}_2 \\ &= (1/3)\begin{pmatrix} \alpha + 2\,\sigma_{11} - \sigma_{22} & 0 & 0 \\ 0 & \alpha - \sigma_{11} + 2\,\sigma_{22} & 0 \\ 0 & 0 & -2\,\alpha - \sigma_{11} - \sigma_{22} \end{pmatrix}. \end{aligned} \tag{10}$$

By inverting this relation, one can obtain the expressions of σ_{11}, σ_{22} and σ_{33} as functions of S_{11}, S_{22} and α

$$\begin{aligned} \sigma_{11} &= 2\,S_{11} + S_{22} - \alpha; \\ \sigma_{22} &= 2\,S_{22} + S_{11} - \alpha; \\ \sigma_{33} &= -\alpha. \end{aligned} \tag{11}$$

The constitutive equations for both material models are summarized by Eqs. (3), (4), (6) and (11). These equations will be combined with the localized necking criteria in order to numerically determine the FLDs.

3. Localized necking criteria

As earlier mentioned, two strain localization approaches are utilized to predict the onset of localized necking: the bifurcation theory, developed by Rudnicki and Rice [2], and the imperfection approach, originally developed by Marciniak and Kuczynski [3] for positive strain paths, and subsequently extended by Hutchinson and Neale [14] to the whole range of strain paths. Consistent with most studies devoted to the prediction of FLDs, the following assumptions are adopted in the current numerical investigations:

- The studied metal sheet is assumed to be thin.
- The mechanical behavior is taken to be incompressible and, hence, the strain component ε_{33} is equal to $-(\varepsilon_{11}+\varepsilon_{22})$.
- The necking band is assumed to remain normal to the sheet plane during straining.

As a consequence of the above assumptions, most of the following governing equations will be recast into a 2D in-plane formulation.

3.1. Bifurcation theory

3.1.1. Main equations governing the bifurcation theory

The sheet is subjected to proportional loading. Consequently, the velocity gradient $\mathbf{G}$, which is equal to $\dot{\boldsymbol{\varepsilon}}$ in this particular case, is given by the following expression:

$$\mathbf{G} = \dot{\boldsymbol{\varepsilon}} = \begin{bmatrix} \dot{\varepsilon}_{11} & 0 & 0 \\ 0 & \rho\,\dot{\varepsilon}_{11} & 0 \\ 0 & 0 & -(1+\rho)\,\dot{\varepsilon}_{11} \end{bmatrix}, \tag{12}$$

where ρ is the strain-path ratio ranging from $-1/2$ (uniaxial tensile state) to 1 (equibiaxial tensile state).

As demonstrated earlier in [2] and [19], the bifurcation criterion states that localized necking occurs when the acoustic tensor $\vec{\mathrm{N}}.\vec{\mathcal{L}}.\vec{\mathrm{N}}$ becomes singular. This criterion is mathematically expressed as follows:

$$det\,(\vec{\mathrm{N}}.\vec{\mathcal{L}}.\vec{\mathrm{N}}) = 0, \tag{13}$$

where:

- $\vec{\mathrm{N}} = (\cos\theta, \sin\theta)$ is the unit vector normal to the localization band (where θ is the angle between vector $\vec{\mathrm{N}}$ and the major strain direction).
- $\tilde{\mathcal{L}}$ is the in-plane analytical tangent modulus relating the in-plane velocity gradient $\tilde{\mathbf{G}}$ to the in-plane nominal stress rate $\dot{\tilde{\mathbf{N}}}$:

$$\dot{\tilde{\mathbf{N}}} = \tilde{\mathcal{L}} : \tilde{\mathbf{G}}. \tag{14}$$

The above tangent modulus $\tilde{\mathcal{L}}$ is defined by the following expression:

$$\tilde{\mathcal{L}} = \tilde{\mathbf{L}} - \tilde{\mathbf{L}}_1 - \tilde{\mathbf{L}}_2, \tag{15}$$

where $\tilde{\mathbf{L}}_1$ and $\tilde{\mathbf{L}}_2$ are fourth-order tensors that convey the effect of convective Cauchy stress components. They are expressed in the following index forms (see, e.g., [15]):

$$\begin{aligned} \forall\, i,j,k,l = 1,2: \quad \tilde{L}_{1\ ijkl} &= \frac{1}{2}\left[\delta_{ik}\,\sigma_{lj} + \delta_{il}\,\sigma_{kj}\right]; \\ \tilde{L}_{2\,ijkl} &= \frac{1}{2}\left[\sigma_{ik}\,\delta_{lj} - \sigma_{il}\,\delta_{jk}\right]. \end{aligned} \tag{16}$$

As to tensor $\tilde{\mathbf{L}}$, it designates the in-plane instantaneous modulus relating the in-plane strain rate tensor $\tilde{\dot{\varepsilon}}$ to the Jaumann co-rotational derivative $\tilde{\sigma}^{\mathrm{J}}$ of the in-plane Cauchy stress tensor $\tilde{\sigma}$

$$\tilde{\sigma}^{\mathrm{J}} = \tilde{\mathbf{L}} : \tilde{\dot{\varepsilon}}. \tag{17}$$

By virtue of the coaxiality of the Cartesian base vectors (1, 2) with the principal stress axes (σ_{11},σ_{22}), Eq. (17) reduces to

$$\begin{cases} \sigma^{J}_{11} = \tilde{L}_{11}\,\dot{\varepsilon}_{11} + \tilde{L}_{12}\,\dot{\varepsilon}_{22} \\ \sigma^{J}_{22} = \tilde{L}_{12}\,\dot{\varepsilon}_{11} + \tilde{L}_{22}\,\dot{\varepsilon}_{22} \\ \sigma^{J}_{12} = 2\,\tilde{L}_{S}\,\dot{\varepsilon}_{12}. \end{cases} \tag{18}$$

The components $\tilde{L}_{11}$, $\tilde{L}_{22}$, $\tilde{L}_{12}$ and $\tilde{L}_S$ of the in-plane instantaneous modulus $\tilde{\mathbf{L}}$ will be explicitly expressed for the different behavior models in the following subsections.

3.1.2. Instantaneous modulus for the flow theory

In this case, the expression of $\tilde{\mathbf{L}}$ may be derived starting from an elasto-plastic constitutive framework, in which the elastic deformation is taken into account in addition to its plastic counterpart. The rigid-plastic behavior may be treated as a limiting case of the elasto-plastic behavior, when the Young modulus E tends towards $+\infty$. As established by Hutchinson and Neale [14], the 3D constitutive law of the elasto-plastic flow theory can be expressed by the following index form:

$$\begin{aligned} &\forall i,j = 1,2,3: \\ &\sigma^{\mathrm{J}}_{ij} = \frac{2E}{3}\left[\dot{\varepsilon}_{ij} - \beta\, S_{ij}\, S_{kl}\,\dot{\varepsilon}_{kl}\right] + \delta_{ij}\,\mathrm{tr}\left(\boldsymbol{\sigma}^{\mathrm{J}}\right);\ k,l = 1,2,3, \end{aligned} \tag{19}$$

where:

- $\boldsymbol{\sigma}^{J}$ is the Jaumann co-rotational derivative of $\boldsymbol{\sigma}$.
- β is a scalar equal to $(3/(2\,\sigma^2_{eq}))\,(1 - (E_T/E))$.
- E_T is the tangent modulus equal to $d\sigma_{eq}/d\varepsilon_{eq}$. For the particular case of the Hollomon hardening law, E_T is equal to $n\,K\,\varepsilon^{n-1}_{eq}$.
- δ is the Kronecker delta.

Exploiting the fact that σ^{J}_{33} is equal to zero (as σ_{33} is constant during the loading), and by virtue of the incompressibility condition ($\dot{\varepsilon}_{33} = -\dot{\varepsilon}_{11} - \dot{\varepsilon}_{22}$), we can formulate Eq. (19) in the form of Eq. (18). In this case, the following expressions for the components $\tilde{L}_{11}$, $\tilde{L}_{22}$, $\tilde{L}_{12}$ and $\tilde{L}_S$ can be derived:

$$\begin{cases} \tilde{L}_{11} = \dfrac{4}{3}\,E - (E - E_T)\left(\dfrac{2\,S_{11} + S_{22}}{\sigma_{eq}}\right)^2;\ \tilde{L}_{22} = \dfrac{4}{3}\,E - (E - E_T)\left(\dfrac{S_{11} + 2\,S_{22}}{\sigma_{eq}}\right)^2 \\ \tilde{L}_{12} = \dfrac{2}{3}\,E - (E - E_T)\left(\dfrac{(2\,S_{11} + S_{22})(S_{11} + 2\,S_{22})}{\sigma^2_{eq}}\right);\quad \tilde{L}_S = \dfrac{E}{3}. \end{cases} \tag{20}$$

These components $\tilde{L}_{11}$, $\tilde{L}_{22}$, $\tilde{L}_{12}$ and $\tilde{L}_S$ can also be expressed in terms of σ_{11} and σ_{22} as follows:

$$\begin{cases} \tilde{L}_{11} = \dfrac{4}{3}\,E - (E - E_T)\left(\dfrac{\sigma_{11} + \alpha}{\sigma_{eq}}\right)^2;\quad \tilde{L}_{22} = \dfrac{4}{3}\,E - (E - E_T)\left(\dfrac{\sigma_{22} + \alpha}{\sigma_{eq}}\right)^2 \\ \tilde{L}_{12} = \dfrac{2}{3}\,E - (E - E_T)\left(\dfrac{(\sigma_{11} + \alpha)(\sigma_{22} + \alpha)}{\sigma^2_{eq}}\right);\quad \tilde{L}_S = \dfrac{E}{3}. \end{cases} \tag{21}$$

The expressions above for the components $\tilde{L}_{11}$, $\tilde{L}_{22}$, $\tilde{L}_{12}$ and $\tilde{L}_S$ may be viewed as extension of the developments carried out by Hutchinson and Neale [14], which are only valid under the plane stress assumption.

3.1.3. Instantaneous modulus for the deformation theory

To obtain the expression of $\tilde{\mathbf{L}}$ for the J_2 deformation theory of plasticity, the developments of Hutchinson and Neale [14] will be adapted to the case when σ_{33} is different from zero (but remains constant during deformation). In this case, the components $\tilde{L}_{11}$, $\tilde{L}_{22}$, $\tilde{L}_{12}$ and $\tilde{L}_S$ are given by the following relations:

$$\begin{cases} \tilde{L}_{11} = \dfrac{4}{3}\,E_S - (E_S - E_T)\left(\dfrac{2\,S_{11} + S_{22}}{\sigma_{eq}}\right)^2; \\ \tilde{L}_{22} = \dfrac{4}{3}\,E_S - (E_S - E_T)\left(\dfrac{S_{11} + 2\,S_{22}}{\sigma_{eq}}\right)^2 \\ \tilde{L}_{12} = \dfrac{2}{3}\,E_S - (E_S - E_T)\left(\dfrac{(2\,S_{11} + S_{22})(S_{11} + 2\,S_{22})}{\sigma^2_{eq}}\right);\quad \tilde{L}_S = \dfrac{E_S}{3} + Q, \end{cases} \tag{22}$$

where scalar Q is defined as follows:

$$Q = \frac{1}{3}E_S[(\varepsilon_{11} - \varepsilon_{22})\coth(\varepsilon_{11} - \varepsilon_{22}) - 1]. \tag{23}$$

Similar to Eq. (21), the components of $\tilde{\mathbf{L}}$ given in Eq. (22) can be formulated in terms of σ_{11}, σ_{22} and pressure α as follows:

$$\begin{cases} \tilde{L}_{11} = \dfrac{4}{3}\,E_S - (E_S - E_T)\left(\dfrac{\sigma_{11} + \alpha}{\sigma_{eq}}\right)^2;\ \tilde{L}_{22} = \dfrac{4}{3}\,E_S - (E_S - E_T)\left(\dfrac{\sigma_{22} + \alpha}{\sigma_{eq}}\right)^2 \\ \tilde{L}_{12} = \dfrac{2}{3}\,E_S - (E_S - E_T)\left(\dfrac{(\sigma_{11} + \alpha)(\sigma_{22} + \alpha)}{\sigma^2_{eq}}\right);\quad \tilde{L}_S = \dfrac{E_S}{3} + Q. \end{cases} \tag{24}$$

3.1.4. Algorithmic treatment

By analyzing the expression of the in-plane analytical tangent modulus $\tilde{\mathcal{L}}$, and its different components for each plasticity theory, one can easily notice that this modulus is a function of the following parameters and variables: hardening parameters K and n, major strain ε_{11}, strain-path ratio ρ, and pressure α. On the other hand, vector $\vec{\mathrm{N}}$ is completely determined once θ is known. Consequently, the acoustic tensor $\vec{\mathrm{N}}.\,\tilde{\mathcal{L}}.\,\vec{\mathrm{N}}$ is dependent on K, n, ρ, ε_{11}, α and θ:

$$\vec{\mathrm{N}}.\,\tilde{\mathcal{L}}.\,\vec{\mathrm{N}} \triangleq \vec{\mathrm{N}}(\theta).\,\tilde{\mathcal{L}}(\mathrm{K}, n, \rho, \varepsilon_{11}, \alpha).\,\vec{\mathrm{N}}(\theta). \tag{25}$$

When K, n and α are known, the acoustic tensor $\vec{\mathrm{N}}.\,\tilde{\mathcal{L}}.\,\vec{\mathrm{N}}$ becomes only dependent on ρ, ε_{11} and θ:

$$\vec{\mathrm{N}}.\,\tilde{\mathcal{L}}.\,\vec{\mathrm{N}} \triangleq \vec{\mathrm{N}}(\theta).\,\tilde{\mathcal{L}}(\rho, \varepsilon_{11}).\,\vec{\mathrm{N}}(\theta). \tag{26}$$

The algorithm developed to numerically determine the FLD is defined by two nested loops:

- For each strain-path ratio ρ ranging from $-1/2$ to 1, with $\Delta\rho = 0.1$.
  - For each band orientation θ ranging from 0° to 90°, at user-defined intervals of 1°.
    - Solve Eq. (13) with respect to its only unknown ε_{11}. The obtained root is referred to as the critical strain ε^{*}_{11} corresponding to the strain-path ratio ρ and to the band orientation θ.

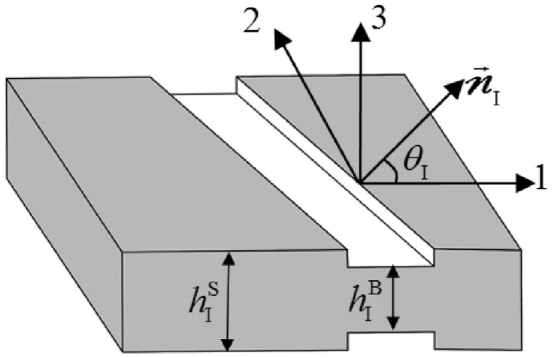

Fig. 2. Illustration of the M–K analysis (initial geometry and band orientation).

The smallest critical strain over all possible band orientations θ and the associated angle define, respectively, the localization limit strain ε_{11}^L and the necking band inclination, which correspond to the strain-path ratio ρ.

3.2. Initial imperfection approach

This approach postulates the preexistence of a small initial imperfection in the form of a narrow band across the sheet (Fig. 2).

The different notations used in Fig. 2 are explained below:

- h_I^B: initial thickness of the band B.
- h_I^S: initial thickness of the safe zone S (outside the band).
- $\vec{N}_I$: initial unit vector normal to the band.
- θ_I: initial band inclination.

3.2.1. Governing equations for the initial imperfection approach

The initial imperfection approach is characterized by the following main equations:

- The kinematic compatibility condition at the interface between the safe zone and the band. This condition allows expressing the jump in the velocity gradient across the band:

$$\widetilde{\mathbf{G}}^B = \widetilde{\mathbf{G}}^S + \dot{\vec{\tilde{c}}} \otimes \vec{\tilde{N}}, \tag{27}$$

where $\vec{\tilde{N}}$ and $\dot{\vec{\tilde{c}}}$ are the current in-plane unit vector normal to the band and the in-plane jump vector, respectively. The velocity gradient in the safe zone $\mathbf{G}^S$ has the same form as in Eq. (12). By inserting Eq. (12) into Eq. (27), one can derive the following expression for $\mathbf{G}^B$:

$$\mathbf{G}^B = \begin{bmatrix} \dot{\varepsilon}_{11} + \dot{c}_1 N_1 & \dot{c}_1 N_2 & 0 \\ \dot{c}_2 N_1 & \rho\,\dot{\varepsilon}_{11} + \dot{c}_2 N_2 & 0 \\ 0 & 0 & -(1+\rho)\,\dot{\varepsilon}_{11} - \dot{c}_1 N_1 - \dot{c}_2 N_2 \end{bmatrix}. \tag{28}$$

- The expressions of the initial and current imperfection ratios denoted by ξ_I and ξ, respectively, and defined by

$$\xi_I = 1 - \frac{h_I^B}{h_I^S}; \quad \xi = 1 - \frac{h^B}{h^S}. \tag{29}$$

The current thickness h^B (resp. h^S) is related to h_I^B (resp. h_I^S) by

$$h^B = h_I^B\, e^{\varepsilon_{33}^B}; \quad h^S = h_I^S\, e^{\varepsilon_{33}^S}, \tag{30}$$

where ε_{33}^B and ε_{33}^S are the 33 components of the logarithmic strain in the band and in the safe zone, respectively. By combining Eqs. (29) and (30), ratios ξ_I and ξ can be related by the following equation:

$$\xi = 1 - (1 - \xi_I)\, e^{(\varepsilon_{33}^B - \varepsilon_{33}^S)}. \tag{31}$$

- The evolution of the band orientation:

$$\mathrm{Tan}(\theta) = e^{(\varepsilon_{11}^S - \varepsilon_{22}^S)}\,\mathrm{Tan}(\theta_I) = e^{(1-\rho)\varepsilon_{11}^S}\,\mathrm{Tan}(\theta_I). \tag{32}$$

Table 1
Hardening parameters for the used materials.

Low-carbon steel (annealed)		304 stainless steel (annealed)	
K (MPa)	n	K (MPa)	n
600	0.21	1400	0.43

- The equilibrium balance at the interface between the safe zone and the band:

$$h^B \widetilde{\boldsymbol{\sigma}}^B \cdot \vec{\tilde{N}} = h^S \widetilde{\boldsymbol{\sigma}}^S \cdot \vec{\tilde{N}}. \tag{33}$$

- The through-thickness normal stress is assumed to be the same in both zones B and S. This allows simplifying the following analysis. Furthermore, this prescribed stress component is taken to be negative and kept constant during straining:

$$\sigma_{33}^B = \sigma_{33}^S = -\alpha \quad \text{with pressure } \alpha \geq 0. \tag{34}$$

- The constitutive equations describing the mechanical behavior, as detailed in Section 2.

3.2.2. Algorithmic treatment

The generic algorithm used to numerically determine the FLD is based on the following three nested loops:

- For each strain-path ratio ρ ranging between $-1/2$ and 1, with $\Delta\rho = 0.1$.
  - For each initial band orientation θ_I spanning the admissible range of inclination angles (i.e., between 0° and 90°), at user-defined intervals of 1°.
    - For each time increment $[t_k, t_{k+1}]$, integrate the governing equations detailed in Section 2 by applying an implicit incremental algorithm very similar to the one developed and used in [15]. The application of this incremental integration scheme is continued until satisfying the following criterion:

$$\dot{\varepsilon}_{33}^B / \dot{\varepsilon}_{33}^S \geq 10. \tag{35}$$

The strain component ε_{11}^S, thus obtained once criterion (35) is satisfied, is considered to be the critical strain ε_{11}^* corresponding to the current band inclination θ and to the strain-path ratio ρ.

The smallest critical strain, over all initial angles θ_I, solution of the previous algorithm defines the necking limit strain ε_{11}^L corresponding to the strain-path ratio ρ.

4. Numerical predictions and results

In this section, numerical predictions are carried out for two steel grades: the annealed low-carbon steel (shortly designated in the following "LCS") and the annealed 304 stainless steel (called shortly hereafter "304SS"). The hardening parameters for these grades are defined in Table 1.

To better emphasize the difference between the mechanical responses of LCS and 304SS, the stress–strain responses for both steel grades are displayed in Fig. 3.

The remainder of this section is divided into two main sections; the first corresponds to the results obtained by the application of the bifurcation theory, while the second contains the results yielded by the initial imperfection approach.

4.1. Bifurcation theory predictions

Before analyzing the influence of pressure α on the onset of bifurcation for the whole range of strain paths, attention is first confined to the particular case of plane strain state ($\rho = 0$). In this case, the evolution of the limit strain ε_{11} versus pressure α is plotted in Fig. 4(a). For this particular strain path, the limit strain computed on the basis of the flow

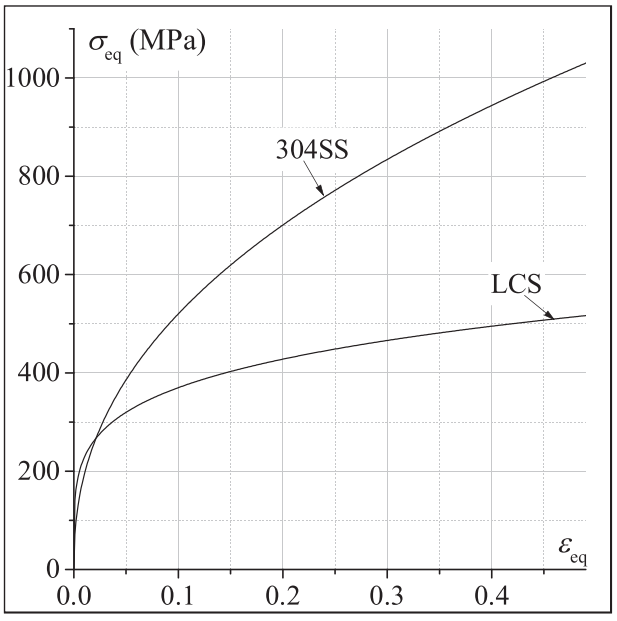

Fig. 3. Stress–strain curves: comparison between low-carbon steel and 304 stainless steel.

theory is exactly the same as that yielded by the deformation theory, irrespective of the steel grade and pressure level. This preliminary observation generalizes the results reported in [14] and [15], which were only established for the particular case of plane stress conditions. It is also found that the limit strain is equal to the value of the hardening exponent n when pressure α is equal to 0 (which corresponds to a plane stress state). This result is quite expectable and can also be recovered by the Hill criterion [7]. From Fig. 4, it is revealed that ε_{11} increases with pressure α. In order to better understand the effect of pressure α on the limit strain ε_{11}, the bifurcation condition given by Eq. (13) is further developed for the case of plane strain tension. In this particular case, the necking band orientation θ is equal to 0°, as demonstrated in several investigations (see, for instance, [14] and [15]), and confirmed in the current work through numerical predictions. Hence, the unit normal vector $\tilde{\tilde{\mathrm{N}}}$ is equal to (1, 0). Consequently, Eq. (13) reduces to the following equation:

$$det\,(\mathbf{C}) = 0 \quad \text{where} \quad \forall\, i,j = 1,2\colon C_{ij} = \tilde{\mathcal{L}}_{1ij1}. \tag{36}$$

From Eq. (36), and considering the previously derived expressions for the analytical tangent modulus, the components C_{12} and C_{21} are equal to 0. Consequently, $det\,(\mathbf{C})$ is equal to the product $C_{11}C_{22}$. After some straightforward derivations, components C_{11} and C_{22} can be expressed in the following form:

$$\begin{aligned} C_{11} &= \alpha + 3^{-\frac{(1+n)}{2}}\, 2^{1+n} \left(\frac{n}{\varepsilon_{11}} - 1\right) K\, \varepsilon_{11}^{n}; \\ C_{22} &= 2^{-1+n}\, 3^{-\frac{(1+n)}{2}}\, K\, \varepsilon_{11}^{n} \left(1 + \coth\left(\varepsilon_{11}\right)\right). \end{aligned} \tag{37}$$

As clearly shown in Eq. (37) $_2$, component C_{22} is always strictly positive (as $\varepsilon_{11} > 0$) and independent of pressure α. Hence, the onset of bifurcation corresponds to the vanishing of component C_{11}:

$$C_{11} = 0 \Leftrightarrow \varepsilon_{11} = \frac{n}{1 - 3^{\frac{1+n}{2}} 2^{-1-n} \frac{\alpha}{K\,\varepsilon_{11}^{n}}}. \tag{38}$$

For the studied case of plane strain tension, the equivalent stress σ_{eq} is related to the strain component ε_{11} by the following equation:

$$\sigma_{eq} = K\, \frac{2^{n}}{3^{\frac{n}{2}}} \varepsilon_{11}^{n}. \tag{39}$$

The insertion of Eq. (39) into Eq. (38) leads to the following expression:

$$C_{11} = 0 \Leftrightarrow \varepsilon_{11} = \frac{n}{1 - \frac{\sqrt{3}}{2} \frac{\alpha}{\sigma_{eq}}}. \tag{40}$$

From Eqs. (38) and (40), one can easily observe that ε_{11} increases with pressure α. Therefore, Eq. (38) shows the sensitivity of the evolution of the limit strain ε_{11} as a function of pressure α to the adopted sheet metal parameters K and n. By analyzing Eq. (38) and comparing the curves of Fig. 4(a), one can easily conclude that the limit strain of the low-carbon steel is more affected by the level of pressure α than the limit strain of 304 stainless steel is. This result is also expectable, considering the difference in the hardening behavior of the two steel grades (see Fig. 3). Indeed, for a given equivalent strain, the equivalent stress of the LCS material is lower than that of the 304SS material. This reveals that the impact of pressure α on σ_{eq} is more important for the 304SS than for the case of LCS. To further emphasize this aspect, the evolution of ε_{11} as a function of pressure α normalized by σ_{eq} is displayed in Fig. 4(b). The resulting evolution is almost the same for both alloys, which confirms the observation made on Fig. 4(a).

It has been observed in practice that applying a normal pressure during forming of a sheet improves its formability. This effect is successfully captured by numerical predictions, as demonstrated in Fig. 5,

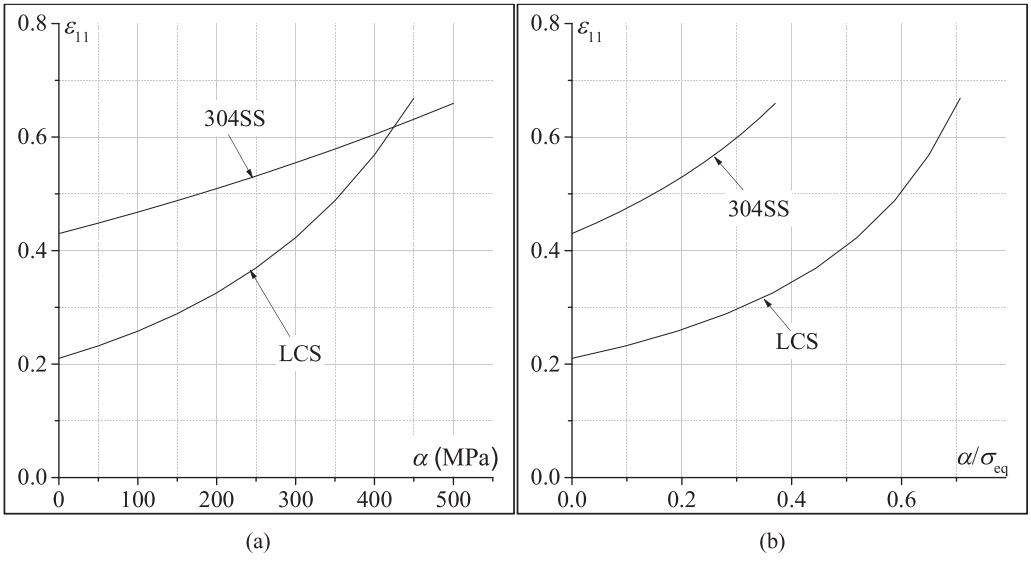

Fig. 4. Evolution of the limit strain ε_{11} (for plane strain tension) as a function of: (a) pressure α, (b) ratio α/σ_{eq}.

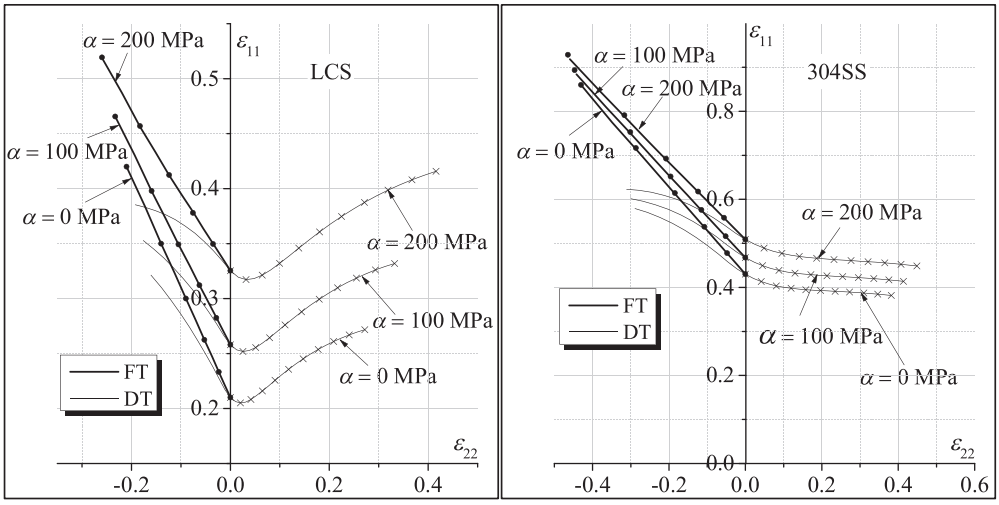

Fig. 5. Effect of pressure α on the FLDs, as obtained by bifurcation theory: (a) LCS; (b) 304SS.

where simulations are performed with different values for the normal pressure: 0 MPa (which corresponds to a plane stress state), 100 MPa, and 200 MPa. This figure confirms, and extends to other strain paths, the observation that the limit strains of low-carbon steel are more sensitive to the amount of normal pressure α than those of 304 stainless steel, as already observed in Fig. 4 for the plane strain tension loading path. Other important conclusions, pertaining to each of the adopted constitutive frameworks, may be drawn on the basis of these simulation results:

- *Flow theory of plasticity*: bifurcation cannot occur in the biaxial tension range ($\rho > 0$), irrespective of the steel grade and pressure level. In the negative ρ range, however, bifurcation is predicted at realistic levels of limit strains. In order to validate our numerical predictions, the well-known Hill criterion [7], which is valid in its original form under the plane stress assumption, is generalized in the present case to a more general stress state that includes a non-zero normal stress. After some lengthy derivations detailed in Appendix A, the following analytical relation is obtained for the limit strain (major strain):

$$\varepsilon_{11} = \frac{2^{n+1}\varepsilon_{11}^{n}\, K\, n\, (\rho^2+\rho+1)^{\frac{n+2}{2}}}{-3^{\frac{n+1}{2}}\alpha\,(\rho+1)^2\sqrt{\rho^2+\rho+1} + 2^{n+1}\varepsilon_{11}^{n}\, K\,(\rho+1)\,(\rho^2+\rho+1)^{\frac{n+2}{2}}}. \tag{41}$$

Usually, the values of parameters K, n, ρ and α are fixed and, hence, Eq. (41) may be viewed as a non-linear equation for the principal unknown ε_{11}. This limit strain ε_{11} can then be determined by solving this equation with an iterative procedure. The associated minor strain ε_{22} is simply computed by multiplying the obtained solution ε_{11} by ρ. The FLDs determined by solving the analytical Eq. (41) are represented in Fig. 5 by dotted graphs with symbols (•). One can easily verify from this figure that the numerical predictions follow exactly the solution of the analytical formula (41). This comparison proves the suitability and the accuracy of the proposed numerical tools.

By analyzing Eq. (41), one can observe that, when pressure α is different from 0, the limit strain ε_{11} (and hence ε_{22}) depends on the material parameters K, n as well as on the strain-path ratio ρ. This is a main difference with the case of a plane stress state, where the limit strain only depends on ρ and n. Eq. (41) also reveals that the impact of pressure α on the limit strain is more important for low values of K and/or n. This remark provides another justification to the fact that the limit strain of low-carbon steel grade is more sensitive to the amount of pressure α than the limit strain of 304 stainless steel grade.

When pressure α is set to 0 (which corresponds to the case of plane stress state), the well-known Hill formula is obviously recovered from Eq. (41)

$$\varepsilon_{11} = \frac{n}{(\rho+1)}. \tag{42}$$

For plane strain tension ($\rho = 0$), and for a general stress state ($\alpha \neq 0$), the following equation can be readily derived from Eq. (41):

$$\varepsilon_{11} = \frac{2^{n+1}\varepsilon_{11}^{n}\, K\, n}{-3^{\frac{n+1}{2}}\alpha + 2^{n+1}\varepsilon_{11}^{n}\, K}. \tag{43}$$

By fixing the values of the hardening parameters K and n, one can establish from Eq. (43) a non-linear relation between the limit strain ε_{11} and pressure α. Therefore, one can plot the evolution of ε_{11} as a function of α. This evolution is identical to that already reported in Fig. 4.

- J_2 *deformation theory*: unlike the flow theory, the application of the J_2 deformation theory in conjunction with the bifurcation approach leads to finite and realistic limit strains in the biaxial tension range ($\rho > 0$). For negative strain paths ($\rho < 0$), the limit strains computed by the deformation theory are always lower than their counterparts predicted by the flow theory. The equality of the limit strains predicted by both plasticity theories is only observed for the case of plane strain tension. Similar to the case of flow theory, the application of normal pressure α increases the limit strain when the deformation theory is used as behavior model. To more closely analyze the influence of pressure α on the level of the limit strain ε_{11}, Eq. (13) is further developed for positive strain paths ($\rho > 0$). Similar to the case of plane strain tension ($\rho = 0$), the necking band orientation θ is equal to 0° for positive strain paths. This result is also confirmed in the current work through numerical predictions. Hence, vector $\vec{\mathrm{N}}$ is equal to (1, 0), which allows the following analytical relation to be derived from criterion (13):

$$-3^{\frac{n+1}{2}}\alpha\,(\rho^2+\rho+1)^2 + 2^{n-1}K\,\varepsilon_{11}^{n-1}\,(\rho^2+\rho+1)^{\frac{n+1}{2}}\big(-3\,\rho^2 - n\,(\rho+2)^2 + 2\,\varepsilon_{11}(\rho+2)(\rho^2+\rho+1)\big) = 0. \tag{44}$$

The limit strain ε_{11} can then be determined by solving the non-linear Eq. (44) via an iterative numerical scheme. The forming limit diagrams obtained by solving Eq. (44) are provided in Fig. 5 (dotted graphs with symbol ×). By comparing the right-hand side of the FLDs reported in Fig. 5, it is clear that the FLDs based on Eq. (44) are identical to those given by the numerical tool developed in Section 3, which provides an additional validation for the latter.

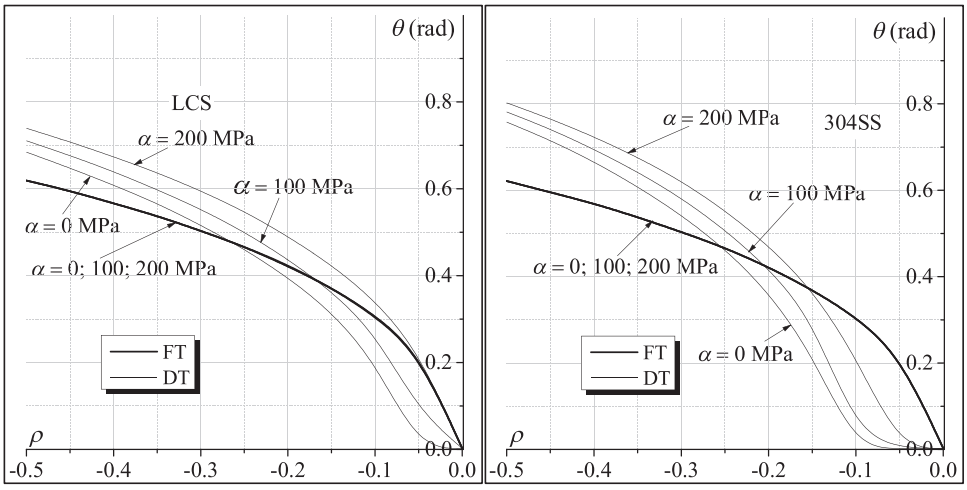

Fig. 6. Effect of pressure α on the plots of necking band orientation θ versus strain-path ratio ρ, as determined by the bifurcation theory: (a) LCS; (b) 304SS.

Moreover, in the particular case of plane stress state ($\alpha = 0$), Eq. (44) provides directly the associated limit strain in the following form:

$$\varepsilon_{11} = \frac{3\,\rho^2 + n\,(\rho+2)^2}{2\,(\rho+2)(\rho^2+\rho+1)}. \tag{45}$$

Eq. (45) above is the well-known Stören and Rice formula [19], which provides the major limit strain at localized necking based on the deformation theory of plasticity in conjunction with plane stress conditions.

Again, an observation similar to that made in the case of flow theory applies here. Indeed, the limit strain ε_{11} associated with a non-zero normal pressure ($\alpha \neq 0$, see Eq. (44)) depends on ρ, K and n, while it only depends on ρ and n in the case of plane stress state (see Eq. (45)).

The plots of the necking band orientation θ versus the strain-path ratio ρ are displayed in Fig. 6 for both plasticity theories (i.e., flow theory and deformation theory of plasticity). Note that for $\rho < 0$, the inclination of the band θ, which results from the analysis, is that minimizing the critical strain ε^*_{11} for all possible band orientations. For the positive ρ range, it is demonstrated from the different simulations that the necking band orientation θ is always equal to 0° for the deformation theory, while no bifurcation is predicted when the flow theory is used. Consequently, the plots of localization band angle θ are only presented in the negative ρ range (see Fig. 6). The above observations hold true regardless of the value of pressure α. For both theories of plasticity, the necking band orientation increases with the absolute value of the strain-path ratio ρ. In the case of the deformation theory, the value of this band orientation is dependent on the amount of pressure α, and it increases with the latter (the lowest value of band orientation being obtained in the case of plane stress state ($\alpha = 0$)). However, when the flow theory is applied, the necking band inclination θ reveals to be independent of α. In this latter case, one can easily verify through numerical simulations that θ is related to ρ by the following formula:

$$\theta = \arctan\sqrt{-\rho}, \tag{46}$$

which is exactly the same formula as that given by Hill's localized necking analysis [7], within the framework of rigid-plastic flow theory and plane stress conditions. This result is an additional validation of our developed numerical tools.

The analytical and numerical results established in this section for the case of constant normal stress, on the basis of bifurcation theory, will be extended in Appendix B to the case of variable normal stress, which is taken proportional to the equivalent stress.

4.2. M–K analysis predictions

Before examining in detail the effect of normal pressure α for the whole range of strain paths, attention is first focused on the particular case of plane strain tension ($\rho = 0$). For this particular strain path, the initial orientation θ_I for the necking band is equal to 0° (i.e., the one that minimizes the limit strain over all possible initial band inclinations). Using the update Eq. (32), it is easy to demonstrate that the necking band orientation θ remains equal to 0° during straining. Consequently, the normal vector $\vec{\mathrm{N}}$ keeps its initial value (1, 0) all along loading. Hence, the equilibrium Eq. (33) reduces to the following scalar equation:

$$h^B\,\sigma^B_{11} = h^S\,\sigma^S_{11}. \tag{47}$$

It is also well known that, for this particular loading path of plane strain tension, the strain path remains proportional during deformation both in the band and in the safe zone (see, e.g., [14]). Accordingly, $\boldsymbol{\varepsilon}^B$ and $\boldsymbol{\varepsilon}^S$ can be expressed in the following generic forms:

$$\boldsymbol{\varepsilon}^B = \begin{pmatrix} \varepsilon^B_{11} & 0 & 0 \\ 0 & 0 & 0 \\ 0 & 0 & -\varepsilon^B_{11} \end{pmatrix}; \quad \boldsymbol{\varepsilon}^S = \begin{pmatrix} \varepsilon^S_{11} & 0 & 0 \\ 0 & 0 & 0 \\ 0 & 0 & -\varepsilon^S_{11} \end{pmatrix}. \tag{48}$$

The corresponding equivalent strains ε^B_{eq} and ε^S_{eq} are easily obtained from Eq. (48)

$$\varepsilon^B_{eq} = \sqrt{(2/3)\,\boldsymbol{\varepsilon}^B : \boldsymbol{\varepsilon}^B} = \frac{2}{\sqrt{3}}\,\varepsilon^B_{11};$$
$$\varepsilon^S_{eq} = \sqrt{(2/3)\,\boldsymbol{\varepsilon}^S : \boldsymbol{\varepsilon}^S} = \frac{2}{\sqrt{3}}\,\varepsilon^S_{11}. \tag{49}$$

Because the prescribed particular loading path (i.e., plane strain tension) results in a strain path that remains linear in both zones, the normality law (3) corresponding to the flow theory and the constitutive Eq. (6) corresponding to the deformation theory become strictly equivalent. In this case, $\mathbf{S}^B$ and $\mathbf{S}^S$ can be related to $\boldsymbol{\varepsilon}^B$ and $\boldsymbol{\varepsilon}^S$, respectively, by the following relations:

$$\mathbf{S}^B = \frac{2}{3}\frac{\sigma^B_{eq}}{\varepsilon^B_{eq}}\boldsymbol{\varepsilon}^B; \quad \mathbf{S}^S = \frac{2}{3}\frac{\sigma^S_{eq}}{\varepsilon^S_{eq}}\boldsymbol{\varepsilon}^S. \tag{50}$$

Because the components ε^B_{22} and ε^B_{22} are equal to zero (see Eq. (48)), it comes from Eq. (50) that

$$S^B_{22} = 0; \quad S^S_{22} = 0. \tag{51}$$

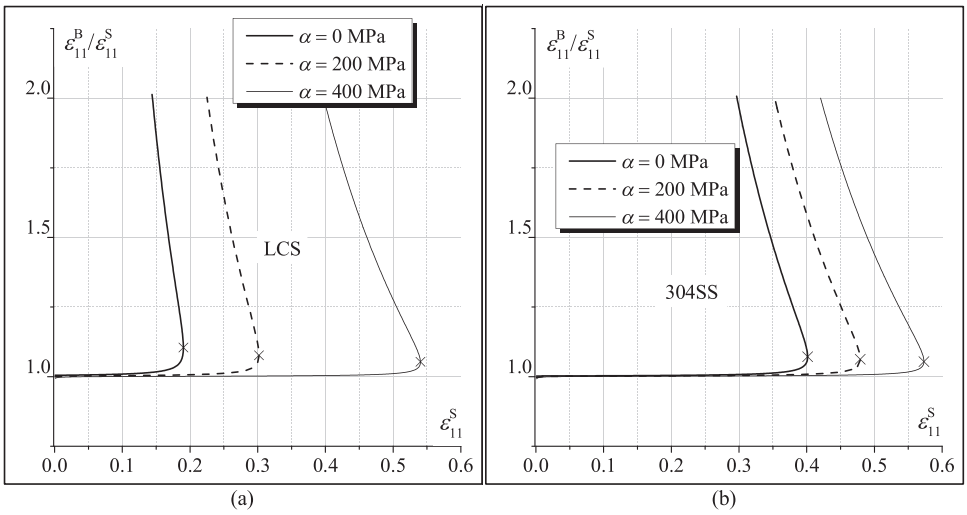

Fig. 7. Evolution of ratio $\varepsilon_{11}^B/\varepsilon_{11}^S$ versus ε_{11}^S for plane strain tension ($\rho=0$, $\xi_I=10^{-3}$): (a) LCS; (b) 304SS.

The combination of the above equation with Eq. (10) allows the expressions of σ_{22}^B and σ_{22}^S to be derived as follows:

$$\sigma_{22}^B = \frac{\sigma_{11}^B - \alpha}{2}; \quad \sigma_{22}^S = \frac{\sigma_{11}^S - \alpha}{2}. \tag{52}$$

Then, the equivalent stresses σ_{eq}^B and σ_{eq}^S are expressed in the following forms:

$$\begin{aligned} \sigma_{eq}^B &= \sqrt{\alpha^2 + (\sigma_{11}^B)^2 - \sigma_{11}^B\,\sigma_{22}^B + (\sigma_{22}^B)^2 + \alpha\,(\sigma_{11}^B + \sigma_{22}^B)} \\ \sigma_{eq}^S &= \sqrt{\alpha^2 + (\sigma_{11}^S)^2 - \sigma_{11}^S\,\sigma_{22}^S + (\sigma_{22}^S)^2 + \alpha\,(\sigma_{11}^S + \sigma_{22}^S)}. \end{aligned} \tag{53}$$

Substituting Eq. (52) into Eq. (53) leads to the following expressions:

$$\sigma_{eq}^B = \frac{\sqrt{3}}{2}(\sigma_{11}^B + \alpha); \quad \sigma_{eq}^S = \frac{\sqrt{3}}{2}(\sigma_{11}^S + \alpha), \tag{54}$$

which are equivalent to

$$\sigma_{11}^B = \frac{2}{\sqrt{3}}\sigma_{eq}^B - \alpha; \quad \sigma_{11}^S = \frac{2}{\sqrt{3}}\sigma_{eq}^S - \alpha. \tag{55}$$

Using the Hollomon hardening law (4) and Eqs. (49), (55) can also be rewritten in the following form:

$$\begin{aligned} \sigma_{11}^B &= \left(\frac{2}{\sqrt{3}}\right)^{n+1} K\,(\varepsilon_{11}^B)^n - \alpha; \\ \sigma_{11}^S &= \left(\frac{2}{\sqrt{3}}\right)^{n+1} K\,(\varepsilon_{11}^S)^n - \alpha. \end{aligned} \tag{56}$$

The following form of the equilibrium equation can be obtained by inserting the above expressions for σ_{11}^B and σ_{11}^S into Eq. (47):

$$h^B\left(\left(\frac{2}{\sqrt{3}}\right)^{n+1} K\,(\varepsilon_{11}^B)^n - \alpha\right) = h^S\left(\left(\frac{2}{\sqrt{3}}\right)^{n+1} K\,(\varepsilon_{11}^S)^n - \alpha\right). \tag{57}$$

Taking into account Eqs. (29), (31) and (48), the equilibrium Eq. (57) can be rearranged as follows:

$$(1-\xi_I)e^{-\varepsilon_{11}^B}\left(\left(\frac{2}{\sqrt{3}}\right)^{n+1} K\,(\varepsilon_{11}^B)^n - \alpha\right) = e^{-\varepsilon_{11}^S}\left(\left(\frac{2}{\sqrt{3}}\right)^{n+1} K\,(\varepsilon_{11}^S)^n - \alpha\right). \tag{58}$$

The strain component ε_{11}^B is varied between 0 and 1, with an increment size of 10^{-3}. For each strain value ε_{11}^B, Eq. (58) is solved by using an iterative procedure, thus providing the corresponding value of ε_{11}^S. The evolution of ratio $\varepsilon_{11}^B/\varepsilon_{11}^S$ versus the strain component ε_{11}^S is plotted in Fig. 7 for different values of normal pressure α. In these simulations, the initial imperfection factor ξ_I is set to 10^{-3}. The crosses marked on the different curves indicate the maximum value that can be reached for ε_{11}^S. This value also corresponds to the limit strain ε_{11}. The different curves reported in Fig. 7 indicate that the predicted limit strain increases with the normal pressure α. This result, which is demonstrated here for the particular case of plane strain tension, will be confirmed and generalized in what follows to the whole range of strain paths.

The combined effect of initial geometric imperfection ratio ξ_I and of pressure α on the evolution and the level of the limit strain ε_{11} is analyzed through the curves of Fig. 8. The results reported in this figure, using the M–K approach, confirm the analyses carried out in Fig. 4, on the basis of bifurcation theory: namely, pressure α enhances the ductility of both steel grades. Moreover, it is again revealed that this enhancement is more significant for low-carbon steel than it is for 304 stainless steel. This difference is due to the contrast in the hardening parameters (Table 1) and, hence, in the stress–strain response (Fig. 3). Furthermore, an increase in the initial imperfection ratio ξ_I leads to a reduction in the level of limit strain ε_{11}.

The evolution of the critical strain ε_{11}^* versus the band orientation θ, which corresponds to the current band inclination determined at the onset of strain localization, for uniaxial tension strain path ($\rho=-0.5$) is displayed in Fig. 9 for different values of pressure α. The initial imperfection ratio ξ_I is set to 10^{-2} for the different simulations. The crosses reported on the different curves indicate the value of the limit strain ε_{11} and the associated necking band orientation. As can be noticed from Fig. 9, the critical strains predicted by the flow theory are more sensitive to the value of the band orientation than are those determined by the application of the deformation theory. This observation is valid whatever the amount of pressure α. Also, the value of the necking band orientation θ seems to very slightly increase with pressure α when the flow theory is applied along with the M–K analysis, as reflected by Fig. 9(a) and (c). This observation marks a slight difference with the result obtained when the bifurcation theory is used in conjunction with the flow theory. Indeed, in this latter case, it was demonstrated (see Fig. 6) that the necking band orientation θ is independent of the value of pressure α. On the other hand, the increase in the necking band orientation with pressure α is more noticeable when the deformation theory is used (see Fig. 9(b) and (d)). This increase in the necking band orientation with the applied pressure, revealed by the M–K analysis, is fully consistent with the results obtained with the bifurcation theory (see Fig. 6).

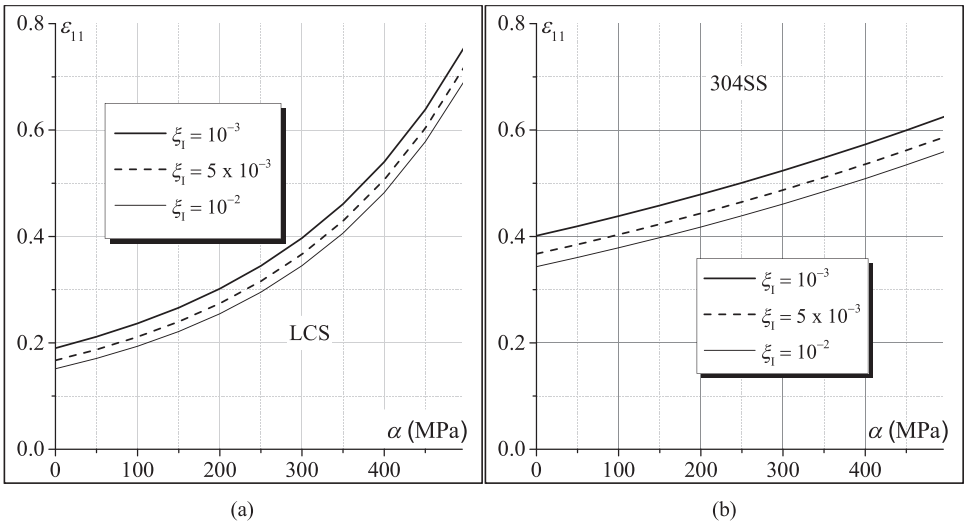

Fig. 8. Evolution of ε_{11} versus pressure α for plane strain tension ($\rho = 0$), as predicted by the M–K analysis: (a) LCS; (b) 304SS.

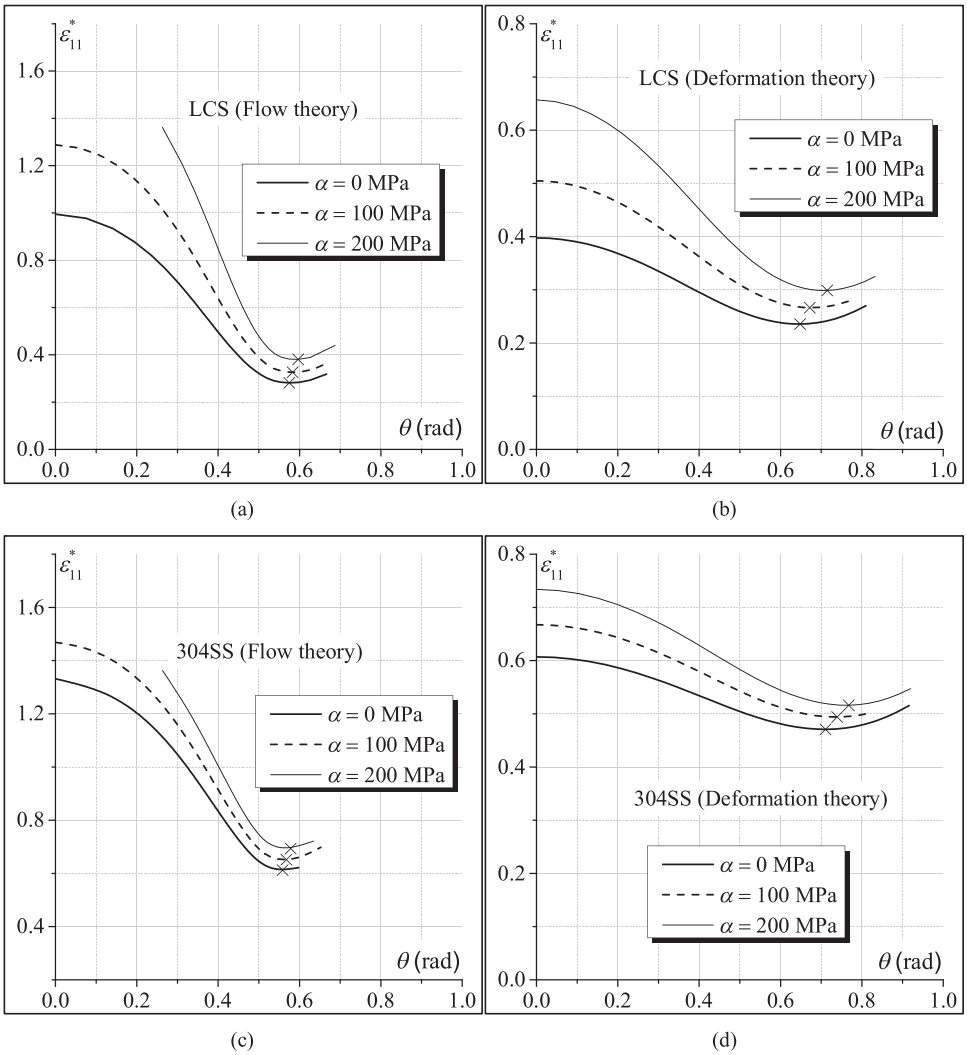

Fig. 9. Evolution of the critical strain ε^*_{11} versus the necking band orientation θ for uniaxial tension strain path ($\rho = -0.5$), as predicted by the M–K analysis ($\xi_I = 10^{-2}$): (a) LCS (Flow theory); (b) LCS (Deformation theory); (c) 304SS (Flow theory); (d) 304SS (Deformation theory).

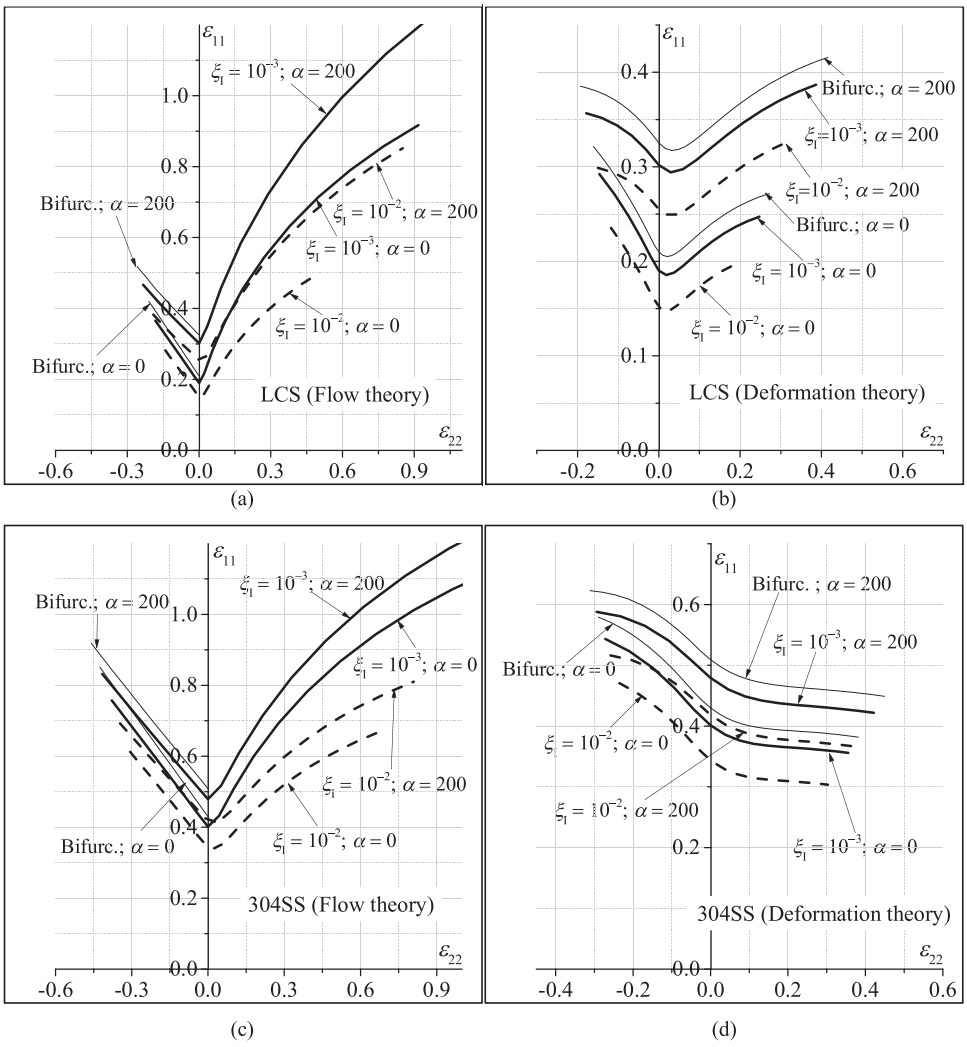

Fig. 10. Effect of pressure α on the predicted FLDs: (a) LCS (Flow theory); (b) LCS (Deformation theory); (c) 304SS (Flow theory); (d) 304SS (Deformation theory).

The respective effects of pressure α and of initial imperfection ratio ξ_I on the shape and location of the predicted FLDs are reflected in Fig. 10. More specifically, comparisons between the predictions given by both plasticity theories are shown with two amounts of pressure: 0 and 200 MPa, and two values for ξ_I: 10^{-3} and 10^{-2}. The predictions obtained with the initial imperfection approach are also compared with those yielded by the bifurcation theory. Four main conclusions may be drawn in view of the presented simulation results:

- As revealed from Fig. 10, which is also consistent with the intermediate results already shown for some particular strain paths, the larger the applied normal pressure α, the higher the limit strains. This result is valid for both plasticity theories and whatever the value of initial imperfection ξ_I.
- For a given amount of normal pressure prescribed to the sheet metal, the limit strain decreases with the size of the initial imperfection ratio. Again, this result holds true whatever the amount of applied normal pressure, and is valid for both plasticity theories, namely flow theory and deformation theory of plasticity.
- In the range of positive strain paths, plastic strain localization occurs at realistic strain levels when predicted based on the deformation theory of plasticity, which is not the case when the flow theory is adopted as constitutive framework. This is made possible thanks to the yield-surface vertex structure inherent in the use of the deformation theory of plasticity.
- It is found that the FLD predicted by bifurcation theory sets an upper limit to the FLDs obtained with the initial imperfection analysis. Moreover, this result is valid for both plasticity theories, and whatever the amount of prescribed normal pressure α. Indeed, Fig. 10 demonstrates that the limit strains computed by the M–K approach tend towards those determined by bifurcation theory when the size of initial imperfection ξ_I tends towards zero. In other words, the effect of an increase in the amount of initial imperfection is essentially to shift the FLD downwards. Considering the similarity in the mathematical formulation of the two strain localization criteria, this trend is quite expectable: the initial imperfection approach obviously reduces to the bifurcation analysis if the amount of initial imperfection is set to zero. This conclusion is valid irrespective of the value of pressure α.

To further validate the developed numerical tools, we compare in what follows our predictions with the results published by Wu et al. [20]. In this latter work, the considered sheet metal was assumed to be isotropic with rate-independent elasto-plastic behavior. Also, the Young modulus E, the Poisson ratio ν and the hardening parameters K and n have been set to 500, 0.3, 3 and 0.22, respectively. The Marciniak–Kuczynski imperfection analysis has been used to predict the onset of localized necking. For the application of this approach, the initial imperfection ratio ξ_I has been set to 10^{-2}. To compare the results reported in [20] with our numerical predictions, we use the modeling approach based on the coupling between the rigid-plastic flow theory and the initial imperfection analysis. The hardening parameters and the initial imperfection ratio taken as inputs in our simulations are the same as those used in [20]. It must be noted that, contrary to the model used in [20],

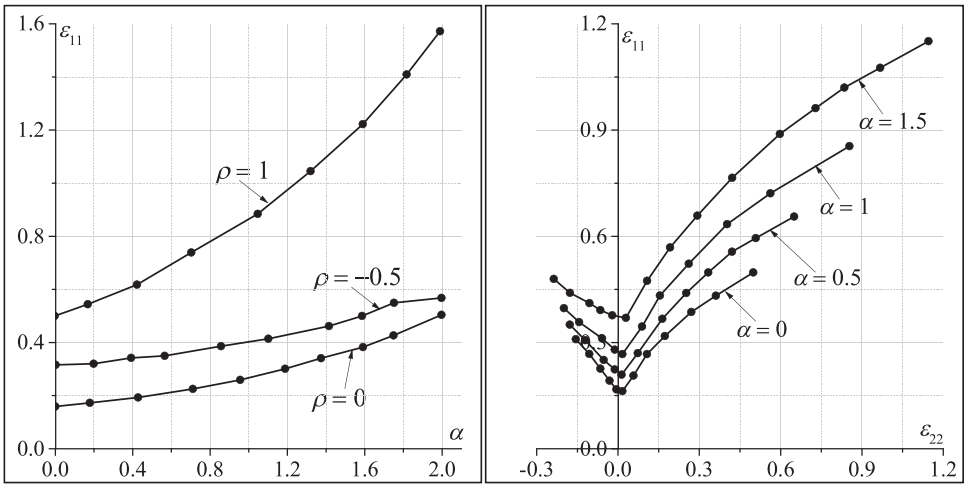

Fig. 11. Comparison between the numerical results reported in [20] and our numerical predictions: (a) Effect of normal stress α on the limit strain ε_{11} for three strain paths ($\rho = -0.5$, $\rho = 0$ and $\rho = 1$); (b) Effect of normal stress α on the FLDs.

elasticity is neglected in our constitutive modeling. This choice is justified by the fact that strain localization occurs at relatively large strains. The suitability of this choice will be discussed hereafter. The comparisons between our numerical predictions and the results reported in [20] are shown in Fig. 11. The solid lines represent the results obtained by our numerical tool, while the dotted graphs with symbol (●) correspond to those published in [20]. It is clear that both results match perfectly, which provides additional validations of our developed numerical tools. Furthermore, the perfect correspondence between our predictions and those presented in [20] confirms that the impact of elasticity on the predictions of localized necking is negligible, which justifies our choice of rigid-plastic constitutive framework.

5. Conclusions

Various theoretical and numerical tools have been developed in this paper in order to thoroughly analyze the influence of through-thickness normal compressive stress on the onset of plastic strain localization in thin metal sheets. For the sake of comparison, the mechanical behavior of the studied sheet metals has been taken to follow the flow theory or, alternatively, the deformation theory of plasticity. In the same way, in order to allow for various cross comparisons, the initiation of plastic strain localization is predicted using both the bifurcation theory and the initial imperfection approach. The main conclusions based upon the current investigation may be summarized as follows:

- The developed theoretical and numerical tools, based on the coupling of two localized necking criteria with two constitutive theories of plasticity, predict an increase in the formability limit with compressive normal stresses. This trend confirms the results obtained in earlier contributions from the literature. Therefore, compressive normal stresses may be used advantageously to effectively avoid the initiation of early localized necking in sheet metal forming.
- The various numerical results show a more significant increase in terms of formability limits when the values of hardening parameters are relatively small.
- When the size of the initial imperfection involved in the M–K imperfection analysis tends towards zero, the corresponding FLDs tend towards the bifurcation-based FLD. This result is valid for both plasticity theories and whatever the value of pressure α.
- Several cross comparisons with some analytical expressions and formulas, specifically derived for the prediction of localized necking, served as additional validations for the proposed numerical tools.

Appendix A. Extension of Hill's localized necking criterion to non-zero constant out-of-plane compressive stress state

It has been theoretically demonstrated in [5] that out-of-plane stress, even as small as one tenth of the yield stress, may notably raise the forming limit strain. In the latter work, the classical Hill localized necking criterion was applied within the J_2 rigid-plastic flow theory of plasticity. Also, isotropic hardening has been modeled by the Hollomon hardening law (identical to Eq. (4)). The authors have demonstrated in [5] that the major strain ε_{11} and the minor strain ε_{22} are related, at the onset of localized necking, by the following relation:

$$\varepsilon_{11} + \varepsilon_{22} = \frac{n}{1-\beta}, \tag{A.1}$$

where scalar β is expressed as follows:

$$\beta = \frac{1}{2}\frac{m'\,(2\,m' + m + 1)}{(m^2 - m + 1) + m'\,(m' + m + 1)}. \tag{A.2}$$

As to factors m and m', these are given by the following expressions:

$$m = \frac{\sigma_{22}}{\sigma_{11}}; \quad m' = -\frac{\sigma_{33}}{\sigma_{11}} = \frac{\alpha}{\sigma_{11}}. \tag{A.3}$$

The expressions of σ_{11} and σ_{22} can be derived by making use of Eqs. (3), (4) and (11)

$$\begin{aligned}
\sigma_{11} &= \frac{-\alpha\sqrt{\rho^2+\rho+1} + 3^{-\frac{n+1}{2}}\,2^n K\,(\rho+2)\,\varepsilon_{11}^n\,(\rho^2+\rho+1)^{\frac{n}{2}}}{\sqrt{\rho^2+\rho+1}} \\
\sigma_{22} &= \frac{-\alpha\sqrt{\rho^2+\rho+1} + 3^{-\frac{n+1}{2}}\,2^n K\,(2\,\rho+1)\,\varepsilon_{11}^n\,(\rho^2+\rho+1)^{\frac{n}{2}}}{\sqrt{\rho^2+\rho+1}}.
\end{aligned} \tag{A.4}$$

The insertion of expressions (A.4) for the stress components σ_{11} and σ_{22} into Eq. (A.3) provides the following forms of factors m and m':

$$\begin{aligned}
m &= \frac{-\alpha\sqrt{\rho^2+\rho+1} + 3^{-\frac{n+1}{2}}\,2^n K\,(2\,\rho+1)\,\varepsilon_{11}^n\,(\rho^2+\rho+1)^{\frac{n}{2}}}{-\alpha\sqrt{\rho^2+\rho+1} + 3^{-\frac{n+1}{2}}\,2^n K\,(\rho+2)\,\varepsilon_{11}^n\,(\rho^2+\rho+1)^{\frac{n}{2}}} \\
m' &= \frac{\alpha\sqrt{\rho^2+\rho+1}}{-\alpha\sqrt{\rho^2+\rho+1} + 3^{-\frac{n+1}{2}}\,2^n K\,(\rho+2)\,\varepsilon_{11}^n\,(\rho^2+\rho+1)^{\frac{n}{2}}}.
\end{aligned} \tag{A.5}$$

By inserting the above expressions of m and m' into Eq. (A.2), factor β can be expressed as follows:

$$\beta = \frac{2^{-n-1}\,3^{\frac{n+1}{2}}\,\alpha\,(\rho+1)\,\varepsilon_{11}^{-n}\,(\rho^2+\rho+1)^{-\frac{n}{2}}}{K\sqrt{\rho^2+\rho+1}}. \tag{A.6}$$

Table A.1
Specialization of the different equations to the particular case of a plane stress state.

Equation	Plane stress form
(A.1)	$\varepsilon_{11}+\varepsilon_{22}=n$
(A.2)	$\beta=0$
(A.3)	$m=\sigma_{22}/\sigma_{11}$; $m'=0$
(A.4)	$\sigma_{11}=\frac{3^{-\frac{n+1}{2}}2^n K(\rho+2)\varepsilon_{11}^n(\rho^2+\rho+1)^n}{\sqrt{\rho^2+\rho+1}}$; $\sigma_{22}=\frac{3^{-\frac{n+1}{2}}2^n K(2\rho+1)\varepsilon_{11}^n(\rho^2+\rho+1)^n}{\sqrt{\rho^2+\rho+1}}$
(A.5)	$m=\frac{2\rho+1}{\rho+2}$; $m'=0$
(A.8), (A.9)	$\varepsilon_{11}=n/(1+\rho)$

For linear strain paths, ε_{22} is related to ε_{11} by the following relation:

$$\varepsilon_{11}=\rho\,\varepsilon_{22}. \tag{A.7}$$

The combination of Eqs. (A.1) and (A.7) gives

$$\varepsilon_{11}=\frac{n}{(1-\beta)(1+\rho)}. \tag{A.8}$$

The insertion of expression (A.6) for factor β into Eq. (A.8) allows obtaining the final analytical expression for ε_{11}

$$\varepsilon_{11}=\frac{2^{n+1}\varepsilon_{11}^n\,\mathrm{K}\,n\,(\rho^2+\rho+1)^{\frac{n+2}{2}}}{-3^{\frac{n+1}{2}}\alpha\,(\rho+1)^2\sqrt{\rho^2+\rho+1}+2^{n+1}\varepsilon_{11}^n\,\mathrm{K}\,(\rho+1)\,(\rho^2+\rho+1)^{\frac{n+2}{2}}}. \tag{A.9}$$

In order to further emphasize the impact of pressure α on the main equations of this Appendix, Table A.1 summarizes the form of these equations in the particular case of a plane stress state ($\alpha=0$).

Appendix B. Extension of the bifurcation approach to the case of variable normal stress

In the previous sections, we assumed that the prescribed normal pressure is constant and independent of the evolution of the stress state during the deformation. In fact, we made this assumption because it accurately describes the stress state involved in hydroforming processes (sheet hydroforming or tube hydroforming). Indeed, during these forming processes, the applied fluid pressure is assumed to be constant during the loading. This assumption has been adopted in several investigations devoted to the prediction of forming limit diagrams by the M–K approach (see, e.g., [11,12,17,18]). The validity of this assumption, in the context of hydroforming processes, has been checked by comparing the numerical predictions with the experimental results (see, e.g., [11,12,17,18]). However, this assumption seems to be inappropriate for other forming processes, such as deep-drawing or single incremental forming processes. Indeed, the normal stress σ_{33} is generally dependent on the stress state in these processes. This stress component is generally assumed to be proportional to the in-plane major stress σ_{11} (see, e.g., [8,9]) or to the equivalent stress σ_{eq} (see, e.g., [10,13]). In the previous investigations, which considered that the normal stress component evolves during the deformation, it has been mostly demonstrated that this normal stress enhances formability. To enlarge the numerical investigations carried out in the previous sections, we extend here the developed numerical tools by assuming that the normal stress may proportionally evolve as a function of the equivalent stress σ_{eq}. To this end, we introduce the normalized normal stress parameter γ, which can be defined as the ratio of the opposite of the normal stress to the equivalent stress ($-\sigma_{33}/\sigma_{eq}$). Similar to the case of constant out-of-plane stress, both localization criteria (namely, the bifurcation theory and the M–K approach) are applied here within the two constitutive frameworks (namely, the flow theory and the deformation theory of plasticity).

When the bifurcation approach is used in conjunction with the deformation theory of plasticity, the following relation can be derived from the bifurcation criterion (13):

$$\varepsilon_{11}=\frac{\sqrt{3}\,(3\rho^2+n(\rho+2)^2)}{2(1+\rho+\rho^2)(2\sqrt{3}+\sqrt{3}\rho-3\gamma\sqrt{1+\rho+\rho^2})}. \tag{B.1}$$

It must be noted that Eq. (B.1) is only applicable to the range of positive strain paths ($\rho\geq 0$), where the necking band orientation θ is equal to 0. This Eq. (B.1) may be viewed as the counterpart of Eq. (44) in the case of variable normal stress. When parameter γ is set to 0 (which corresponds to the particular case of plane stress state), Eq. (45) is obviously recovered.

We extend in what follows Hill's localized necking criterion to the case of variable out-of-plane compressive stress state (which is the counterpart of the developments carried out in Appendix A for constant normal stress). In this case, factors m and m' (see Eq. (A.4)) are given by the following expressions:

$$m=\frac{\sigma_{22}}{\sigma_{11}};$$

$$m'=-\frac{\sigma_{33}}{\sigma_{11}}=\frac{2^n 3^{-\frac{n}{2}}\gamma\,K\varepsilon_{11}^n\left(\rho^2+\rho+1\right)^{\frac{n}{2}}}{\sigma_{11}}. \tag{B.2}$$

The stress components σ_{11} and σ_{22} are given by the following equations (the counterpart of Eq. (11)):

$$\sigma_{11}=2\,S_{11}+S_{22}-\gamma\sigma_{eq};$$

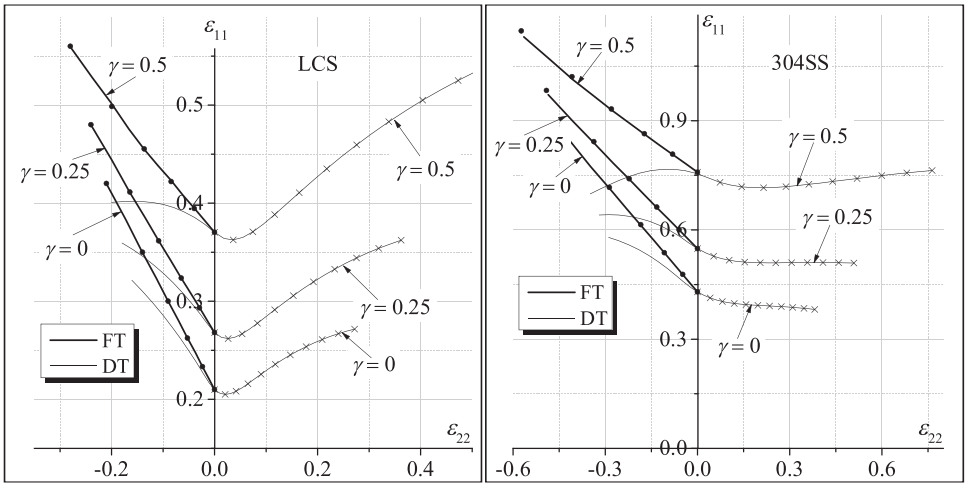

(a) (b)

Fig. B.1. Effect of parameter γ on the FLDs, as obtained by bifurcation theory: (a) LCS; (b) 304SS.

$$\sigma_{22} = 2\,S_{22} + S_{11} - \gamma\sigma_{eq}. \tag{B.3}$$

By using Eqs. (3) and (4), these stress components can be expressed after some straightforward calculations as

$$\begin{aligned}\sigma_{11} &= 2^n\,3^{-\frac{2+n}{2}}\,\mathrm{K}\varepsilon_{11}^n(\rho^2+\rho+1)^{\frac{n-1}{2}}\left(\sqrt{3}\,(\rho+2) - 3\gamma\sqrt{\rho^2+\rho+1}\right)\\ \sigma_{22} &= 2^n\,3^{-\frac{2+n}{2}}\,\mathrm{K}\varepsilon_{11}^n(\rho^2+\rho+1)^{\frac{n-1}{2}}\left(\sqrt{3}\,(2\rho+1) - 3\gamma\sqrt{\rho^2+\rho+1}\right).\end{aligned} \tag{B.4}$$

By inserting the above expressions of σ_{11} and σ_{22} into Eq. (B.2), one obtains

$$\begin{aligned} m &= \frac{\sqrt{3}(2\rho+1) - 3\gamma\sqrt{\rho^2+\rho+1}}{\sqrt{3}(\rho+2) - 3\gamma\sqrt{\rho^2+\rho+1}};\\ m' &= \frac{\sqrt{3}\sqrt{\rho^2+\rho+1}}{(\rho+2) - 3\gamma\sqrt{\rho^2+\rho+1}}.\end{aligned} \tag{B.5}$$

The expression of factor β, introduced in Eq. (A.2), can be put in a more compact form by using Eq. (B.2), which gives

$$\beta = \frac{\sqrt{3}\gamma\,(\rho+1)}{2\sqrt{\rho^2+\rho+1}}. \tag{B.6}$$

The major limit strain ε_{11} can be finally derived by inserting expression (B.6) for factor β into Eq. (A.8)

$$\varepsilon_{11} = \frac{2\sqrt{3}n\sqrt{\rho^2+\rho+1}}{(\rho+1)\left(-3\gamma\,(\rho+1) + 2\sqrt{3}\,\sqrt{\rho^2+\rho+1}\right)}. \tag{B.7}$$

This Eq. (B.7) may be viewed as the counterpart of Eq. (A.9) in the case of variable normal stress. When scalar γ is set to 0, the well-known Hill localized necking criterion is obviously recovered

$$\varepsilon_{11} = \frac{n}{(\rho+1)}. \tag{B.8}$$

By analyzing Eqs. (B.1) and (B.7), one can notice that the limit strain ε_{11} is independent of the hardening parameter K, which is not the case when the normal stress is assumed to be constant (see Eqs. (41) and (44)).

The effect of parameter γ on the limit strains predicted by the bifurcation approach for the whole range of strain paths is shown in Fig. B.1 (which may be viewed as the counterpart of Fig. 5 in the case of variable normal stress). The forming limit diagrams given by Eq. (B.1) (respectively, Eq. (B.7)) are represented by dotted graphs with symbol × (respectively, symbol ●). The results reported in Fig. B.1 confirm the validity of the analytical formulas (B.1) and (B.7).

References

[1] Keeler SP, Backofen WA. Plastic instability and fracture in sheets stretched over rigid punches. Trans ASM 1963;56:25–48.
[2] Rudnicki JW, Rice JR. Conditions for localization of deformation in pressure-sensitive dilatant materials. J Mech Phys Solids 1975;23:371–94.
[3] Marciniak Z, Kuczynski K. Limit strains in the processes of stretch-forming sheet metal. Int J Mech Sci 1967;9:609–20.
[4] Fressengeas C, Molinari A. Instability and localization of plastic flow in shear at high strain rates. J Mech Phys Solids 1987;35:185–211.
[5] Gotoh M, Chung T, Iwata N. Effect of out-of-plane stress on the forming limit strain of sheet metals. JSME Int J Ser A 1995;38:123–32.
[6] Swift H. Plastic instability under plane stress. J Mech Phys Solids 1952;1:1–18.
[7] Hill R. On discontinuous plastic states, with special reference to localized necking in thin sheets. J Mech Phys Solids 1952;1:19–30.
[8] Allwood JM, Shouler DR. Generalised forming limit diagrams showing increased forming limits with non-planar stress states. Int J Plast 2009;25:1207–30.
[9] Fatemi A, Dariani BM. Forming limit prediction of anisotropic material subjected to normal and through thickness shear stresses using a modified M–K model. Int J Adv Manuf Tech 2015;80:1497–509.
[10] Assempour A, Nejadkhaki HK, Hashemi R. Forming limit diagrams with the existence of through-thickness normal stress. Comput Mater Sci 2010;48:504–8.
[11] Zhang F, Chen J, Chen J. Forming limit model evaluation for anisotropic sheet metals under through-thickness normal stress. Int J Mech Sci 2014;89:40–6.
[12] Zhang F, Chen J, Chen J. Effect of through-thickness normal stress on forming limits under Yld2003 yield criterion and M–K model. Int J Mech Sci 2014;89:92–100.
[13] Mirfalah-Nasiri SM, Basti A, Hashemi R. Forming limit curves analysis of aluminum alloy considering the through-thickness normal stress, anisotropic yield functions and strain rate. Int J Mech Sci 2016;116:93–101.
[14] Hutchinson JW, Neale KW. Sheet necking – II. Time-independent behavior. In: Koistinen DP, Wang NM, editors. Mechanics of sheet metal forming. Plenum; 1978. p. 127–53.
[15] Ben Bettaieb M, Abed-Meraim F. Investigation of localized necking in substrate-supported metal layers: comparison of bifurcation and imperfection analyses. Int J Plast 2015;65:168–90.
[16] Eyckens P, Van Bael A, Van Houtte P. Marciniak–Kuczynski type modelling of the effect of through-thickness shear on the forming limits of sheet metal. Int J Plast 2009;25:2249–68.
[17] Hashemi R, Assempour A, Khalil Abad EM. Implementation of the forming limit stress diagram to obtain suitable load path in tube hydroforming considering M–K model. Mater Des 2009;30:3545–53.
[18] Hashemi R, Abrinia K. Analysis of the extended stress-based forming limit curve considering the effects of strain path and through-thickness normal stress. Mater Des 2014;54:670–7.
[19] Stören S, Rice JR. Localized necking in thin sheets. J Mech Phys Solids 1975;23:421–41.
[20] Wu PD, Embury JD, Lloyd DJ, Huang Y, Neale KW. Effects of superimposed hydrostatic pressure on sheet metal formability. Int J Plast 2009;25:1711–25.